ACS APPLIED MATERIALS & INTERFACES

Research Article

www.acsami.org

Wet-Chemical Synthesis and Consolidation of Stoichiometric Bismuth Telluride Nanoparticles for Improving the Thermoelectric Figure-of-Merit

V. Stavila,*[,†] D.B. Robinson,[†] M.A. Hekmaty,[†] R. Nishimoto,[†] D.L. Medlin,[†] S. Zhu,[‡] T.M. Tritt,[‡] and P.A. Sharma*[,§]

[†]Sandia National Laboratories, Livermore, California 94551, United States

[‡]Clemson University, Clemson, South Carolina 29634, United States

[§]Sandia National Laboratories, Albuquerque, New Mexico 87123, United States

Supporting Information

ABSTRACT: Bismuth telluride nanoparticles (NPs) have been synthesized using a low-temperature wet-chemical approach from bismuth(III) oleate and tri-*n*-octylphosphine telluride. The size and shape of the NPs can be controlled by adjusting the temperature, reaction time, and nature of the surfactants and solvents. Aromatic hydrocarbons (toluene, xylenes) and ethers (phenyl- and benzyl-ether) favor the formation of stoichiometric Bi_2Te_3 NPs of platelike morphology, whereas the presence of oleylamine and 1-dodecanethiol yields Bi-rich Bi_2Te_3 spherical NPs. XRD, IR, SEM, TEM, and SAED techniques have been used to characterize the obtained products. We show that the surfactants can be efficiently removed from the surface of the NPs using a two-step process employing nitrosonium tetrafluoroborate and hydrazine hydrate. The surfactant-free NPs were further consolidated into high density pellets using cold-pressing and field-assisted sintering techniques. The sintered surfactant-free Bi_2Te_3 showed electrical and thermal properties comparable to Bi_2Te_3 materials processed through conventional solid state techniques, and greatly improved over other nanostructured Bi_2Te_3 materials synthesized by wet-chemical approaches.

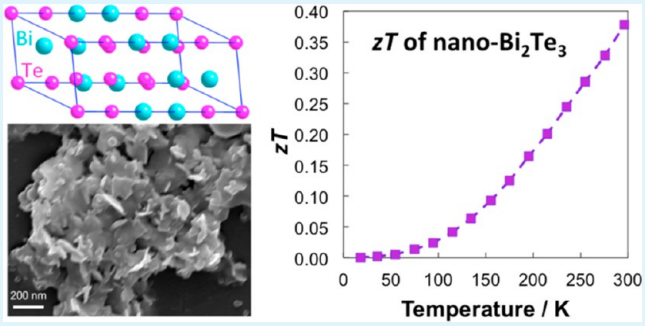

KEYWORDS: *nanoparticles, bismuth telluride, wet-chemical synthesis, surfactants, electrical properties, thermoelectrics*

INTRODUCTION

Bismuth telluride is among the most widely used thermoelectric materials because it displays a dimensionless thermoelectric figure of merit zT close to unity near room temperature. The zT of a material is defined as $zT = S^2\sigma T/\kappa$, where S, σ, κ, and T are the Seebeck coefficient, the electrical conductivity, the thermal conductivity, and the temperature in Kelvin, respectively. The central problem in thermoelectrics is to increase zT in order to achieve higher efficiency thermoelectric (TE) devices. State-of-the-art bulk TE materials used in devices have a $zT \approx 1$,[1,2] whereas materials with $zT > 2$ are required to compete with more widespread refrigeration or thermal energy harvesting technologies. Although many promising TE materials have been discovered in recent years, including oxides, silicides, heuslers, skutterudites, clathrates, etc.,[1,2] bismuth chalcogenide-based materials are still the most widely used.

Previous literature, including both theoretical calculations and experiments, has established that Bi_2Te_3 based materials with nanoscale grain sizes show dramatic improvements in zT.[3−7] It is believed that such improvements originate when grain size becomes less than the phonon mean free path but larger than the electronic mean free path. In this way, the contribution to κ from phonons will decrease, whereas σ and S will largely be unaffected.[6,8] A prevalent technique for reducing grain size involves the milling of large grained materials. However, mechanical milling results in a broad grain size distribution, even after separating out larger grains with a sieve. As a result, nanoparticle (NP) synthesis strategies from the "bottom up" using wet chemical routes are of active interest, and are a plausible path to a bulk material with narrower grain size distribution.

Bismuth telluride NPs have been synthesized using a variety of wet-chemical techniques,[9−17] but there is no general strategy for achieving a narrow size distribution, tailored properties, and desired morphologies. The growth mechanisms for NPs synthesized this way are not well understood. Dirmyer et al. utilized a solution-phase route using long-chain thiols as

Received: April 20, 2013
Accepted: June 27, 2013
Published: June 27, 2013

capping agents to construct relatively monodisperse Bi_2Te_3 NPs at temperatures as low as 50 °C; however, the thiols are difficult to remove, and can interfere with consolidation into a useful product.[16] The metal chalcogenide complex method, which consists of dissolution of a metal chalcogenide (typically a metal sulfide in hydrazine in the presence of excess sulfur) has also been successfully employed to generate $Bi(Sb)_2Te(Se)_3$ NPs, but the method requires significant amounts of anhydrous hydrazine, which is dangerously reactive in the presence of certain catalysts.[10,18,19] Scheele et al. studied the reaction of Bi NPs with TOP-Te and found that spherical ∼10 nm in diameter NPs can be isolated, although the as-synthesized NPs were Bi-rich.[17] Toprak et al. demonstrated the synthesis of bulk amounts of Bi_2Te_3 NPs by reducing co-precipitated Bi and Te oxides at 400 °C;[20] however, gaseous hydrogen is required for the redox reaction, and hot hydrogen gas would present a significant safety hazard if used on a large scale. These methods generally lack control over morphology and size, resulting in particles with a wide particle size distribution or ill-defined microstructures composed of nanoscale polycrystalline domains. Further improvements in zT using such NPs will also require successful consolidation. A secondary problem in this field is that any surfactants involved in synthesis degrade the electrical properties of sintered pellets significantly. Surfactants are difficult to remove from the synthesis as they provide more control over particle size and morphology.

Recently, Hyeon and co-workers[3] and Scheele and co-workers[11] achieved better control over size and morphology of Bi_2Te_3 NPs by reacting bismuth dodecanethiolate and tri-*n*-octylphosphine telluride in the presence of various surfactants. Despite certain advantages over previously reported approaches, both methods employ thiols as surfactants, which are difficult to remove completely from the surface of the NPs.[21,22] The presence of organic surfactants can lead to a carbonaceous residue at the grain boundaries upon high-temperature consolidation, which was shown to have a detrimental effect on the electrical conductivity.[16] Conversely, metal oleates represent suitable alternatives for thiolates and have been previously proven as useful precursors for the synthesis of various metal chalcogenides.[22] Therefore, we decided to explore the utility of bismuth(III) oleate as a precursor for Bi_2Te_3 NPs.

Here we report a simple synthetic approach towards bulk quantities of nanostructured stoichiometric bismuth(III) telluride using commercially available reagents in standard, low-cost surfactant/solvent systems, where the surfactants can be chemically removed at room temperature to facilitate consolidation. We found that reaction of bismuth(III) oleate (produced in situ from triphenylbismuth and oleic acid) with tri-*n*-octylphosphine telluride proceeds under mild heating to generate Bi−Te particles. Because the surfactants and solvents react differently with each of the bismuth and tellurium precursors, a balance can be found, and the stoichiometry can be tuned through the choice and relative quantities of these reagents, and reaction temperature. Lower temperatures are expected to result in smaller grain size, potentially enhancing thermoelectric properties. More weakly coordinating surfactants and solvents are expected to facilitate surfactant stripping, but more strongly coordinating solvents also help to control particle size, so a balance is required. Specifically, we investigated the following aspects of the nanoparticle synthesis and growth: (i) the effects of growth temperature, (ii) variation with surfactants and solvents, (iii) reaction time, and (iv) surfactant removal and particle consolidation. The method is scalable and was used to generate >10 g batches of near-stoichiometric Bi_2Te_3 NPs. These batches are of sufficient size for sintering experiments in commercial field-assisted sintering (FAST) (also known as spark plasma sintering) instruments. We have shown that the surfactant stripping process significantly improves the mechanical and thermoelectric properties of the FAST-consolidated product, resulting in one of the highest zT values for chemically synthesized Bi_2Te_3.

EXPERIMENTAL SECTION

Synthesis. All starting materials and solvents were reagent grade and obtained from commercial sources. The synthetic procedures were conducted under dry, inert Ar atmosphere using Schlenk-line and glove-box techniques.

Preparation of the Bismuth(III) Oleate Solution. Triphenylbismuth (0.881 g, 2.0 mmol) was loaded into a Schlenk flask and evacuated for 30 min, then filled with Ar. Oleic acid (5.2 mL, 7.5 mmol) was added via a syringe and the flask was heated in an oil bath to 80 °C under flowing Ar. The mixture was kept at 80 °C and stirred for 30 min until a transparent viscous solution was obtained.

Preparation of a Stock TOP-Te Solution. The precursor tri-*n*-octylphosphine telluride (TOP-Te) was prepared from a mixture of elemental Te (0.394 g, 3.0 mmol) in 20 mL of neat TOP. First, elemental Te was loaded into a Schlenk flask that was evacuated and then filled with Ar. Next, liquid TOP was transferred to the flask via a syringe and the mixture was heated to 190 °C under vigorous stirring. All elemental Te disappeared in approx. 60 min to form a transparent yellow solution. The temperature of the resulting TOP-Te solution was adjusted to the desired value and used immediately in the reaction with $Bi(oleate)_3$.

General Preparation of Bi−Te NPs. In a typical preparation, the solutions of $Bi(oleate)_3$ and TOP-Te in a stoichiometric (2:3) molar ratio were heated on a silicone oil bath to the set temperature (60, 120, or 180 °C). The TOP-Te was transferred quickly to the Schlenk flask with the Bi(III) precursor via cannula transfer upon stirring. When the effect of additional solvents/surfactants (toluene, xylenes, phenyl ether, benzyl ether, oleylamine and 1-dodecanethiol) was tested, 10 mL of the corresponding organic compound per 1.0 mmol $Bi(oleate)_3$ was used and the reaction was performed overnight (16 h). The Schlenk flask was withdrawn from the bath after various reaction times after the injection and cooled to room temperature. Before the reaction mixture forms a gel, toluene (∼10 mL) was added to the reaction mixture. The Bi−Te product was precipitated with ethanol and washed several times by adding toluene and ethanol followed by centrifugation for 10 min at 8000 rpm. More generally, the Bi−Te NPs can be separated from the reaction mixture by adding excess ethanol, 2-propanol, or acetone to a toluene suspension. Products can be redispersed in toluene, hexanes, and chlorinated solvents, such as $CHCl_3$ and CH_2Cl_2.

Synthesis of Bi NPs. Bismuth oleate is synthesized as described above. 1-Dodecanethiol or oleylamine (20 mL) is added to the flask and the mixture is maintained at 60 °C with vigorous stirring for 16 h during which time a dark product is obtained. The bismuth NPs are isolated by adding ethanol followed by centrifugation at 8000 rpm for 30 min. The NPs can be dispersed in toluene and chlorinated solvents and re-precipitated with ethanol or isopropanol.

Surfactant Removal. The as-synthesized and washed NPs are treated with nitrosonium tetrafluoroborate, then with hydrazine hydrate, and dried in vacuum overnight before being transferred to an Ar-filled glove-box. In a typical procedure, the Bi_2Te_3 NPs synthesized from 2 mmol $Bi(oleate)_3$ and 3 mmol TOP-Te are suspended in about 5 mL of hexanes, then 20 mL of 0.33 M solution of $NOBF_4$ in MeCN is added, followed by stirring the mixture for 30 min. About a ten-fold excess of hexanes is added and the NPs are separated by centrifugation (10 min, 8000 rpm). Next, the product is suspended in 20 mL of hydrazine hydrate/hexane mixture (1:1 volume ratio) and sonicated for 10 min. The remaining organic molecules are

extracted into the organic phase, while the NPs are transferred into the polar phase. The hydrazine hydrate/hexane treatment is repeated two times to remove traces of surfactants, then the product is dried in vacuum and transferred into a glove-box.

Characterization. Carbon, hydrogen, bismuth, and tellurium elemental analyses were performed at the Columbia Analytical Laboratories. Transmission electron microscope (TEM) studies were carried out using a JEOL 2010F instrument, operated at 200 kV and equipped with an Oxford energy-dispersive X-ray spectroscopy detector (EDS) for compositional analysis. Scanning Electron Microscopy (SEM) was performed using a JEOL JSM-6700F field-emission scanning electron microscope. X-ray diffraction (XRD) data were obtained with a powder diffractometer (Empyrean, PANalytical) using unfiltered Cu K_α radiation (λ = 1.5406 Å) at 45 kV and 40 mA. The contribution from $K_{\alpha 2}$ radiation was stripped using a Ni filter. The processing of the powder diffraction results and phase identification was accomplished using HighScore+. The Fourier transform infrared spectra were collected at room temperature using a Varian 800 IR spectrometer in attenuated total reflection (ATR) mode.

Nanoparticle Consolidation. Field-assisted sintering (FAST) experiments were performed using a Dr. Sinter SPS-515S equipped with an analysis unit from Metal Processing Systems. FAST has often been shown to achieve high density compacts while limiting grain growth. Cold pressed powder was generally pressed at 6 tons for 5 minutes using a Carver hydraulic press, further details are provided below. In the FAST method, a relatively large pulsed current is applied through the sample that is contained within a surrounding graphite cylinder while applying pressure with graphite rods. Graphite foil is placed between the sample and the graphite rods in order to keep the sample from sticking to the rods. The foil is easily removed after consolidation. Current is injected into the sample at a constant rate (50 A/min in the present work). Heat is applied to the sample through internal Joule heating and Joule heating in the surrounding graphite cylinder and rods. Nominally DC current is switched on and off over time with a 12:1 ratio over a fixed total hold time (5 minutes in the present work). Two different pressure and temperature conditions were employed. For a pressure of 20 MPa, the holding temperature was 420 °C at a maximum current of 350 A. For a pressure of 40 MPa, a holding temperature of 350 °C was used corresponding to a maximum current of 300 A. The resulting consolidated materials are in the form of 1/2 in. diameter pellets that are typically 2−3 mm in thickness. The resulting pellets are typically densified to greater than 98% of theoretical density.

Electrical and Thermopower Measurements. Hall effect measurements were conducted on consolidated nanoparticles from 2−400 K in a Quantum Design Physical property measurement system. Electroplated Ni and Epo-tek H20B silver epoxy gave Ohmic contacts (linear V−I curves) with low contact resistance (<1 Ω). Hall resistance was linear with magnetic field over the maximum field range of 9 T. Carrier concentration was extracted from the Hall number assuming a Hall factor of 1. Resistivity and Seebeck measurements were performed in a custom designed apparatus described elsewhere[23] from 10 to 300 K. Thermal conductivity measurements were performed in the same temperature range in a separate custom designed system.[24] For thermal conductivity measurements, it is sometimes necessary to perform radiation corrections above $T \approx 220$ K. This was accomplished by subtracting radiative losses based on the sample surface area. Radiative losses as a function of temperature with a temperature gradient along the sample vary to first order as T^3 as derived from the Stefan−Boltzmann law.[25] Two samples of the same batch with different lengths were measured in order to confirm the linear scaling of raw thermal conductivity data with surface area and the use of the T^3 radiation correction factor.

RESULTS AND DISCUSSION

The surfactant choice and experimental conditions are very important during the synthesis of nanostructured bismuth(III) telluride materials. With the wrong choice, products are contaminated with material containing excess elemental Te or Bi. No practical precursors have been reported that start with or enforce the correct Bi_2Te_3 stoichiometry. Because of the layered crystal structure, even when the correct ratio of the elements is used, bismuth can be easily incorporated between the hexagonal planes of the rhombohedral structure, resulting in Bi-rich phases $(Bi_2)_x(Bi_2Te_3)_y$.[26] Despite these perils, we found that Bi(oleate)$_3$ and TOP-Te are suitable precursors for the wet-chemical synthesis of Bi−Te NPs under relatively mild conditions, leading to the appropriate stoichiometry and crystal structure.

Dependence of Particle Structure on Reaction Temperature. The reaction between Bi(oleate)$_3$ and TOP-Te stock solutions was attempted between room temperature and 180 °C. At room temperature, even after several days, no obvious signs of a chemical reaction were observed. When the growth temperature was increased to 60 °C, mixing the Bi and Te precursors resulted in a color change from yellow to dark-brown within several minutes. At 120 and 180 °C, the color change is almost instantaneous. The XRD patterns of the products isolated at 60, 120, and 180 °C are shown in Figure 1

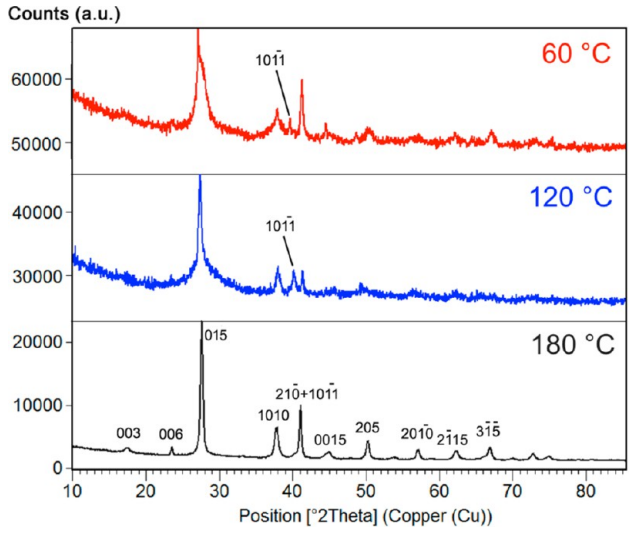

Figure 1. Powder XRD patterns of Bi_2Te_3 synthesized at 60, 120, and 180 °C from bismuth(III) oleate and TOP-Te.

and indicate that a crystalline product is formed, which can be indexed to the rhombohedral crystal system, space group $R\bar{3}m$, characteristic for Bi_2Te_3.[27] Neither elemental bismuth nor tellurium was observed, and this was further confirmed by selective-area electron diffraction (see below). The FWHM of the XRD peaks decrease in the following order 60 < 120 < 180 °C, qualitatively consistent with an increase in the crystallite size for the product synthesized at elevated temperatures.

The Rietveld refinements on the XRD patterns revealed that the crystallite sizes of the products synthesized at 60, 120, and 180 °C are 19, 36, and 95 nm, respectively. Further evidence for the increase in particle sizes upon heating was obtained from SEM (Figure 2A−C) and TEM (Figure 2D−F) measurements. Figure 2A−C shows the SEM images of Bi_2Te_3 NPs synthesized at 60, 120, and 180 °C. At 60 °C, small particles with a diameter of ∼20 nm were obtained, which were relatively round in shape. Figure 2B shows the SEM images of Bi_2Te_3 NPs synthesized at 120 °C and reveals larger particles as well as a change in morphology from spherical NPs to elongated plates. The product isolated at 180 °C (Figure

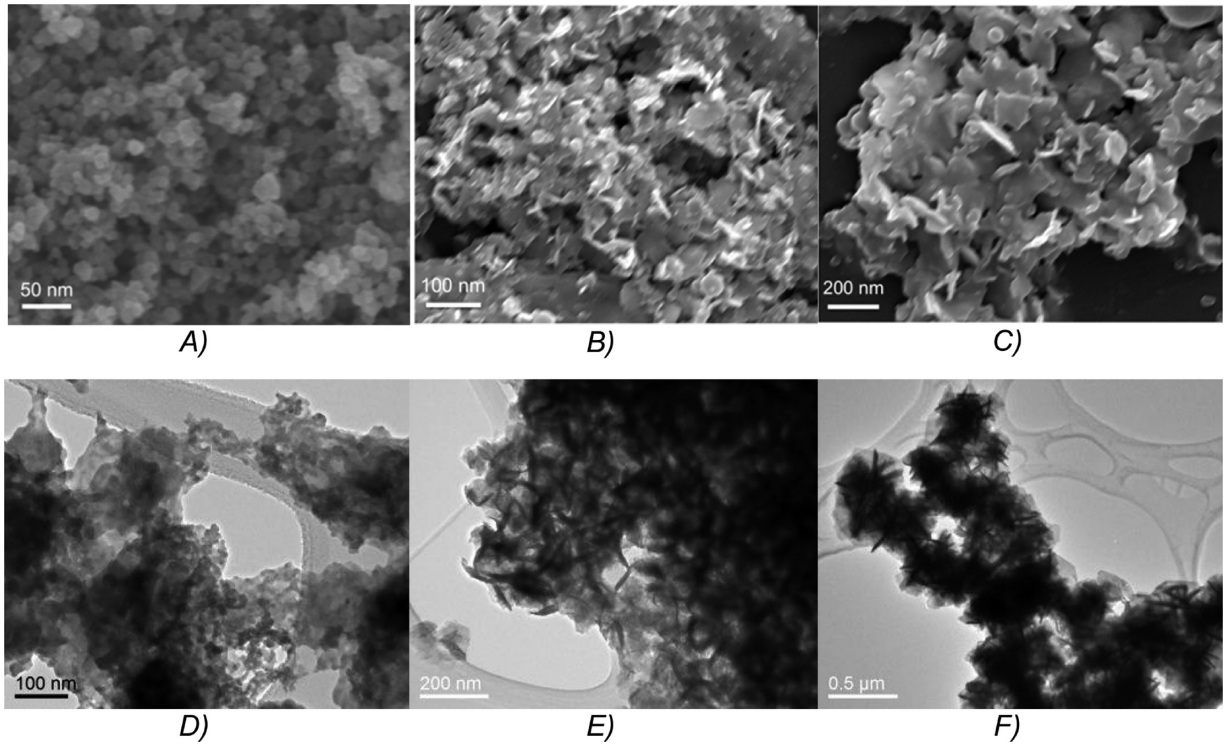

Figure 2. SEM images of Bi_2Te_3 synthesized at (A) 60, (B) 120, and (C) 180 °C and TEM images of Bi_2Te_3 synthesized at (D) 60, (E) 120, and (F) 180 °C.

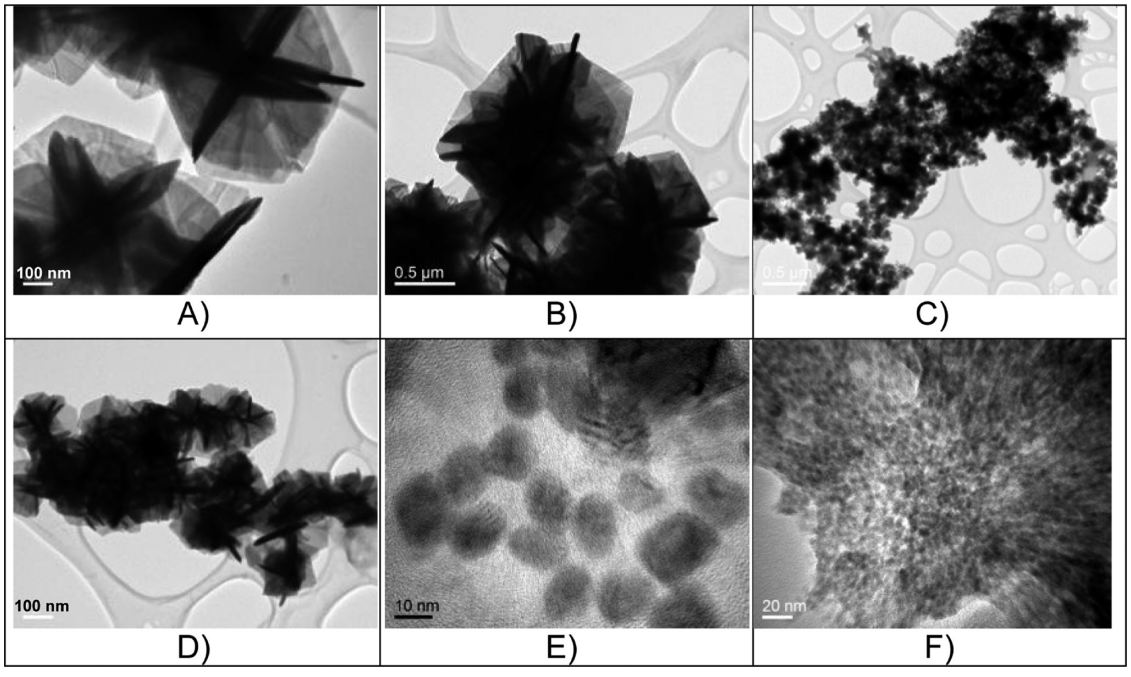

Figure 3. TEM of Bi_2Te_3 synthesized from $Bi(oleate)_3$ and TOP-Te for 16 h in (A) phenyl ether, (B) benzyl ether, (C) toluene, (D) xylenes, (E) oleylamine, (F) 1-dodecanethiol.

2C) displays exclusively platelike morphology. The material consists of inter-grown and agglomerated sub-micrometer assemblies composed of thin plates, tens of nanometers thick and several hundred nanometers long and wide.

The transition from small spherical particles to larger intergrown plates seems to be thermodynamically favorable. The typical size of the NPs obtained at 60 °C observed using TEM (Figure 2D) is similar to the Rietveld refined crystallite size, suggesting the particles are single crystalline. In contrast, the particle size determined from the TEM images of the NPs synthesized at 120 and 180 °C is larger compared to the Rietveld refined values. Similar morphologies were observed for Bi_2Te_3-based nanostructures obtained in solution.[12,28,29]

Dependence of Particle Structure on Solvent and Surfactants. The results above show that the size and structure of Bi_2Te_3 NPs can be controlled by varying the

reaction temperature. We also investigated the effect of various surfactants and solvents on the morphology of the product. Previous work suggests important effects of the surfactants/solvents on morphology of nanostructured Bi_2Te_3 synthesized by sonochemical,[30] hydrothermal,[31,32] solvothermal,[33,34] and solvent-reflux[35] methods. We decided to explore the effect of toluene, xylenes, phenyl ether, benzyl ether, and oleylamine—good solvents for the precursors that have varying polarity, coordinating ability, and reflux temperature—on the morphology and composition of the Bi−Te structures from the $Bi(oleate)_3$ and TOP-Te precursors.

The reaction of $Bi(oleate)_3$ and TOP-Te in benzylether and phenylether at 120 °C resulted in inter-grown plates several hundred nm in diameter and 15-25 nm thick, and agglomerates of the order of several micrometers (Figure 3A-B). These plates are larger than desired, so we considered other reaction conditions to improve upon this. We expect that refluxing solvents may enhance the nucleation of Bi_2Te_3 NPs, resulting in smaller particles. To test this, we performed the synthesis in boiling toluene (111 °C) and xylenes (139 °C). Similar agglomerates to the ethers are formed in boiling xylenes (Figure 3D), suggesting that the reflux conditions do not necessarily play a role in determining the morphology of the resulting NPs. In fact, the morphology of the material isolated with no additional solvent added (Figure 2B, E) is very similar to the products synthesized in toluene and xylenes. Interestingly, the product isolated in boiling toluene (Figure 3C) still displays inter-grown plates as in the case of the aromatic ethers; however, the agglomerates are much smaller, only on the order of a few hundred nanometers in diameter. Xylenes and toluene are similar in terms of their low polarity and coordinating ability, so this result suggests that reaction temperature is the more important parameter.

When oleylamine is added to the reaction mixture prior to TOP-Te, the reaction yields small spherical NPs with a diameter of 15-20 nm (Figure 3E), whereas in the presence of 1-dodecanethiol, spherical particles with a diameter of 8−15 nm are formed. X-ray fluorescence analysis on the sample synthesized in oleylamine showed a bismuth-rich atomic ratio of 4:3, in contrast to the product synthesized in benzyl ether, which is consistent with Bi_2Te_3 (see Figure S1 in the Supporting Information). When the decomposition reaction of $Bi(oleate)_3$ is performed in oleylamine and 1-dodecanethiol with no TOP-Te, small spherical bismuth NPs with a diameter of 10-15 nm are generated (see Figure S2 in the Supporting Information). Scheele et al. showed that similar Bi-rich Bi−Te NPs can be isolated by tellurization of small Bi NPs with TOP-Te in the presence of oleylamine and 1-dodecanethiol.[17]

The reaction of $Bi(oleate)_3$ with TOP-Te in the presence of 1-dodecanethiol and oleylamine is quite distinct compared to reaction in aromatic hydrocarbons. Most notably, the strongly coordinating surfactants lead to reduction of bismuth in addition to formation of the compound. The strong coordination also affects particle size and shape. It is possible that amines and thiols coordinate with no preferred orientation to the Bi_2Te_3 nuclei, slowing and eventually stopping growth, whereas the oxygen atoms of the carboxylate groups favor a specific crystal face, slowing growth on one face but not others, leading to 2D growth.

Similar processes are believed to be responsible for the growth of tellurobismuthinite mineral in nature. Bi_2Te_3 crystals tend to grow along the $a-b$ planes because the covalent bonds within the plane are much stronger than the Te−Te van der Waals bonds along the c direction.[36] The van der Waals gaps separate the Bi_2Te_3 structure into distinct $Te^{(1)}$−Bi−$Te^{(2)}$−Bi-$Te^{(1)}$ penta-atomic sheets along the c axis, referred to as quintuple layers (Figure 4). The weakest bond in the structure

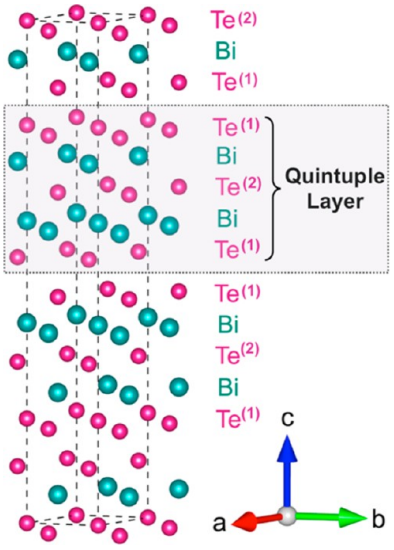

Figure 4. Schematic representation of the quintuple layers in Bi_2Te_3 lattice.

is $Te^{(1)}\cdots Te^{(1)}$ and corresponds to the largest spacing $d \approx 3.7$ Å. During the Bi_2Te_3 crystal growth a free Te atom naturally would have a higher affinity to layers within the basal plane to form a strong covalent bond, whereas van der Waals binding along the c axis is energetically less favorable, and as a result the Te atoms will have a high tendency to grow in the basal plane.

Particle Development with Reaction Time. We also studied the effect of reaction time, in an attempt to gain some insights into the reaction mechanism. We decided to focus on the 120 °C reaction, as in this case the reaction rate proceeds slow enough to isolate many intermediate NP species, yet fast enough to yield small NPs within the range expected for improving TE properties. Benzyl ether was selected as a solvent/surfactant of choice as it results in the highest yield of NPs. The TEM images of the particles isolated upon reacting $Bi(oleate)_3$ and TOP-Te in benzyl ether at 120 °C after 60 sec, 10 min, 30 min and 16 h are presented in Figure 5. Figure 5A, B demonstrates that at the initial stages of the reaction (1 to 10 min) small agglomerated NPs are formed. Electron diffraction patterns are very diffuse, suggesting largely amorphous material. The SAED pattern of the 60 sec sample (Figure 5A) consists of a strong ring of contrast at ~3.25 Å, a second weaker broad ring of contrast at ~1.83 Å and a third very weak broad ring of contrast at ~1.26 Å. The diffuse ring at ~3.25 Å (g=3.08 nm^{-1}) is at the position where the (015) ring of crystalline Bi_2Te_3 should be observed. Since the (015) reflection is the strongest diffraction intensity for crystalline Bi_2Te_3, this may reflect local order consistent with Bi_2Te_3-like coordination. As with the 60 sec sample, the strong diffuse intensity at ~3.23 Å observed for the 10 min sample makes it difficult to see if the strong (015) reflection of Bi_2Te_3 is present. However, the better developed rings at 2.19 Å and 1.81 Å are consistent, respectively, with (110) and (025) Bi_2Te_3 reflections, which are the rings with the next two highest structure factors for the material, and suggest the development of some crystalline material in this specimen.

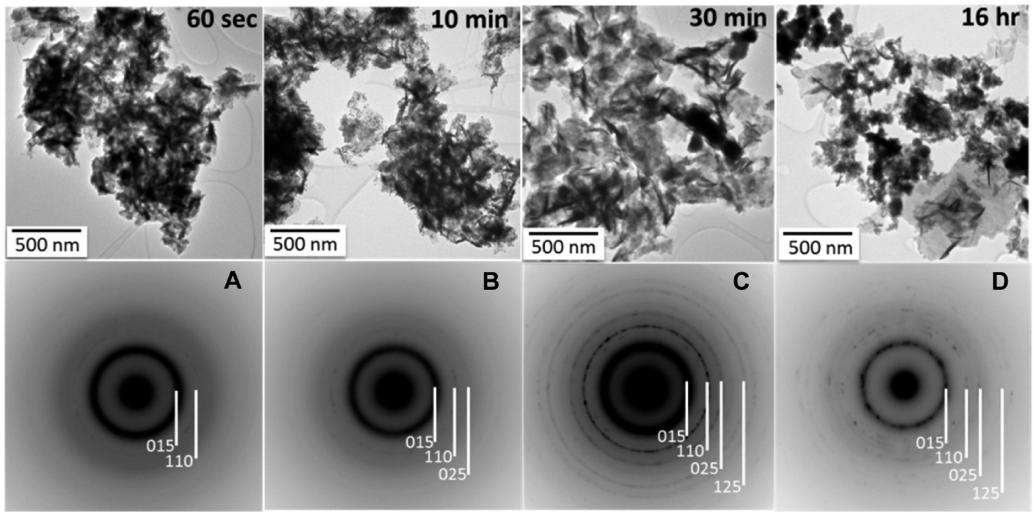

Figure 5. TEM and SAED images of Bi_2Te_3 NPs synthesized from $Bi(oleate)_3$ and TOP-Te in benzyl ether after (A) 60 s, (B) 10 min, (C) 30 min, and (D) 16 h.

The SAED pattern of the 30 min sample suggests it still contains a significant amorphous component, as evidenced by the diffuse ring around 3.23 Å (Figure 5C). Nonetheless, in this sample the development of crystalline material is much clearer than for the 60 second and 10 minute samples. All the strong rings expected for Bi_2Te_3 are present (specifically, (110) d = 2.19 Å; (02-5) d = 1.82 Å; (024) d = 1.61 Å; (030) d = 1.27 Å). Again, the (015) Bi_2Te_3 reflection is ambiguous because it overlaps with the intense diffuse ring at 3.23 Å. Additionally, the 30 min sample has a few spots and partial rings that are distinct from Bi_2Te_3, suggesting the presence of a minor second phase. These include several spots at 2.4 Å, a ring at 1.61 Å, a very faint ring at 1.5 Å, and a few other isolated spots at higher angles. These could be due to traces of crystalline bismuth, although the SAED results cannot afford clear evidence for this. Finally, unlike the other three shorter time samples, the strong diffuse intensity seems to be absent in the SAED pattern of the 16 h sample (Figure 5D) indicating much less of the amorphous material. The SAED pattern is consistent with crystalline Bi_2Te_3. The EDS spectrum of the product confirms the Bi:Te molar ratio in the product is close to 2:3 (see Figure S3 in the Supporting Information).

The growth of bismuth telluride nanocrystals under solvothermal conditions was suggested to occur according to the monoatom model, in which individual Bi and Te atoms are combined to form Bi_2Te_3 nuclei, followed by binding of additional Bi and Te atoms to the initial nucleus during the reaction.[37] Zhao et al. suggested that in some cases a continuous nucleation/nucleus saturation model is also operative.[38] Under the continuous nucleation scenario, the new nuclei of Bi_2Te_3 can form for a long time from the start of the reaction and can continue until all the precursors are completely depleted. We found evidence that at the early stages of the reaction between $Bi(oleate)_3$ and TOP-Te (up to 10 min), the nucleation and growth coexist. After 10 min the cores of the particles start to grow in 2D generating nanoplatelets of Bi_2Te_3 as evidenced by SEM and TEM investigations. After 30 min, the growth is significantly slowed down and essentially is resumed to 2D growth to increase the size of the platelets from tens to hundreds of nanometers.

These results suggest that at the early stages the reaction between bismuth(III) oleate and TOP-Te the formation of small Bi_2Te_3 nuclei occurs. Further NPs growth is strongly dependent on the precursor concentrations and existing surfactants in the system. Alivisatos et al. showed that the newly formed nuclei can either grow by a diffusive mechanism or by aggregation.[39] When sufficient concentrations of the active Bi and Te species are present in solution, the nuclei grow in the high chemical potential environment to form single-crystalline Bi_2Te_3 NPs, possibly via the classical La Mer mechanism.[40] We found that strongly coordinating surfactants produce small round NPs, whereas weakly coordinating surfactants yield large intergrown nanoplates. For Bi_2Te_3 the morphology of particles under conditions close to thermodynamic equilibrium is dependent on the intrinsic crystal structure of the rhombohedral Bi_2Te_3, which favors the growth within the 2D plane of the nanoplates, whereas under conditions far from equilibrium, spherical NPs are generated.

Surfactant Removal and Particle Consolidation. For TE applications that require macroscopic heat and electrical transport, it is important to efficiently remove the organic surfactants from the surface of the NPs to allow for their efficient consolidation. Previous measurements on consolidated NPs that contain surfactants revealed that TE properties are poor because of the low electrical conductivity of the organic molecules or carbonaceous residue at the grain boundaries.[16] Dong et al. reported a general process to chemically remove surfactants at low temperature from various nanocrystals using nitrosonium tetrafluoroborate.[41] We found that the $NOBF_4$ treatment can be successfully applied to Bi_2Te_3 NPs synthesized at 60 °C from $Bi(oleate)_3$ and TOP-Te. During the treatment, it is believed that a ligand exchange process takes place, resulting in NPs stabilized by BF_4^- anions and solvent molecules.[41] $NOBF_4$ was further removed from the surface of the NPs using hydrazine hydrate treatment, which also helps remove the residual organic groups left after the initial $NOBF_4$ treatment. The FTIR spectra of the as-synthesized, $NOBF_4$, and N_2H_4−H_2O-treated NPs are presented in Figure S4 in the Supporting Information. The final material is dried in vacuum overnight and shows no IR features characteristic of organic groups. Elemental analysis confirmed that only traces of carbon are present in dry Bi_2Te_3 NPs after the two-step surfactant removal (Table 1). The dried Bi_2Te_3 NPs have a purity of

98.7%, with only 0.23 wt % C present, so about 99% of the organic material has been removed.

Table 1. Elemental Analysis for the As-Synthesized and $NOBF_4/N_2H_4-H_2O$-Treated Samples

sample	C (wt %)	H (wt %)	Bi (wt %)	Te (wt %)
as-synthesized Bi_2Te_3 NPs	17.95	2.73	42.2	35.5
Bi_2Te_3 NPs with no surfactant	0.23	0.69	53.8	44.9

The new synthetic method is scalable and was used to generate >10 g batches of near stoichiometric Bi_2Te_3 NPs (see Figure S5 in the Supporting Information). We attempted to compact the as-synthesized surfactant-stripped Bi_2Te_3 NPs by cold-pressing and field-assisted sintering (FAST). Cold-pressing of the powder was performed at room temperature in a stainless steel die under various pressures between 5 and 50 MPa. Up to 20 MPa the cold-pressed pellets are mechanically fragile, whereas the powders pressed at 25 MPa and above resulted in dense disks (see Figure S6A in the Supporting Information). However, even the samples cold-pressed at 50 MPa are not sufficiently robust for transport measurements. However, the dry Bi_2Te_3 NPs can be efficiently consolidated with FAST. The samples were pressed in a graphite die applying a pressure of 20 MPa at 420 °C for 5 min. A perfect edge disk was generated that is mechanically robust and can be cleanly fractioned in smaller pieces without cracks or other imperfections. Figure S6B in the Supporting Information shows an optical image of the FAST-consolidated NPs. In the case of FAST particles the measured density of the consolidated NPs is as high as 7.6 g/cm^3, which is 98% of the theoretical Bi_2Te_3 density of 7.7 g/cm^3. The XRD of the consolidated Bi_2Te_3 samples shows an increase in the crystallite size from 24 nm for the powder to 98 nm for the FAST sample (see Figure S7 in the Supporting Information). The low carbon content and the high density of the as-consolidated Bi_2Te_3 NPs makes them promising for TE applications.

Figure 6 compares the electrical properties of our consolidated NPs with and without surfactants, each sintered under 20 MPa at 420 °C for 5 min at an electrical current of 350 A. The surfactant-free sample has both a lower ρ and a higher S over the entire temperature range tested. At room temperature the maximum S value is lower than the value of 120 μV K^{-1} measured by Saleemi et al.,[13] but 1.5 times higher than the value reported by Scheele et al.[17] for nano-Bi_2Te_3. However, the properties of Bi_2Te_3 are strongly dependent upon carrier concentration.[2] The thermal conductivity of the surfactant-free sample is shown at the bottom of Figure 6. A reliable κ measurement could not be achieved in the sample sintered with surfactant because of difficulty obtaining a large enough region of the sample without cracks. For comparison, κ is decomposed into lattice and electronic components. The electronic part of κ was computed using the Wiedemann-Franz law with the temperature-dependent Lorentz number, L, measured for n-type Bi_2Te_3.[42] For example, at room temperature, L = 15.1 nW/Ω K^2. The free electron value of L is 24.4 nW/Ω K^2 and a value of 16.6 nW/Ω K^2 has been reported recently for nanostructured Bi_2Te_3,[43] so our estimate is conservative. The room temperature κ (~2 W/Km) for the surfactant-free sample in Figure 6 is similar to that expected for bulk Bi_2Te_3 with $\rho \approx 1$ mΩ cm.[42]

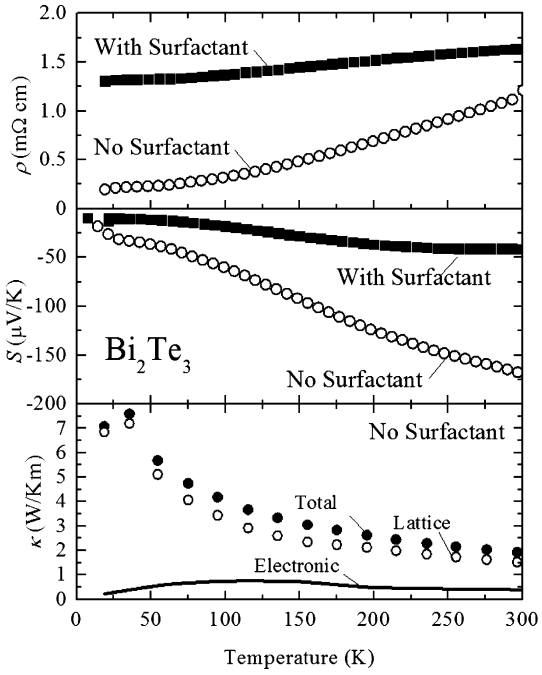

Figure 6. Transport properties of Bi_2Te_3 nanoparticles sintered with and without surfactant. The resistivity (top) and Seebeck coefficient (middle) of consolidated NPs strongly degrade when sintered in the presence of any surfactant. The thermal conductivity of NPs consolidated with a surfactant could not be reliably measured, so only that for NPs sintered without surfactant is shown (bottom).

Tto compare the properties of our Bi_2Te_3 NPs on an equal footing with other Bi_2Te_3 materials, we plot S versus electrical conductivity ($1/\rho$), commonly known as a Jonker plot,[2,44] in Figure 7. For semiconductors, the Jonker plot takes the typical

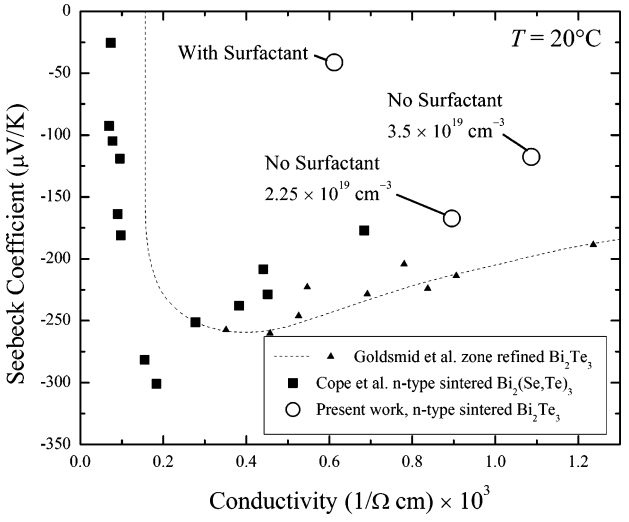

Figure 7. Jonker plot (Seebeck coefficient versus conductivity) at room temperature comparing consolidated Bi_2Te_3 NPs of this work (open circles) with that expected for sintered n-type Bi_2Te_3 (closed squares, ref 46) and zone refined Bi_2Te_3 (closed triangles, ref 45); the dashed line is a guide for the eye. Conductivity is the inverse of resistivity. Samples sintered with and without surfactant are labeled on the plot. Carrier concentrations were measured from the Hall effect for samples consolidated without surfactant. The Hall effect for samples sintered with surfactant was not measured. zT is approximately 0.38 at room temperature for the sample with N = 2.25 × 10^{19} cm^{-3}.

dx.doi.org/10.1021/am401444w | ACS Appl. Mater. Interfaces 2013, 5, 6678−6686

shape of that shown for zone-refined Bi_2Te_3 (dashed line, closed triangles[45]). Carrier concentration is an implicit variable in this plot, where higher carrier concentrations correspond to higher electrical conductivity. A second batch of NPs without surfactant was sintered at 40 MPa, 350 °C, and 300 A, which resulted in a sample with a higher carrier concentration. The two samples we have sintered without surfactants clearly fall on the curve expected for sintered powder Bi_2Te_3 materials (here shown by closed squares,[46] and doped with Se). Note that the samples without surfactant follow the correct trend, where higher carrier concentration leads to higher conductivity, and a commensurate reduction in S as expected from the literature values. The sample sintered with surfactant clearly falls well outside of the line defined by ref 46, where at the same conductivity as n-type Bi_2Te_3, S is much lower. The consolidated NP samples with $N \approx 2.3 \times 10^{19}$ cm^{-3} and $N \approx 3.5 \times 10^{19}$ cm^{-3} had $zT \approx 0.38$ and $zT \approx 0.24$, respectively. These values are consistent with that expected for single crystal[47] and ball-milled/FAST consolidated[48] Bi_2Te_3 samples. The values for κ at room temperature for the surfactant-free samples can also be placed on a Jonker-type plot of κ versus electrical conductivity, and agree well with bulk Bi_2Te_3.[42] The mobility for the sample shown in Figure 7 was ~150 cm^2/V s at room temperature, which is consistent with bulk polycrystalline Bi_2Te_3. Therefore, we have achieved smaller grain sizes in sintered material without a drop in mobility. Finally, because Bi_2Te_3 is amenable to considerable doping manipulation, significant improvements in zT could be achieved.

Evidently, the smallest grain size achieved in this work did not result in a noticeable reduction in κ. Many authors report reductions in κ for Bi_2Te_3 at grain sizes 50 nm or less through ball milling followed by FAST consolidation, which is supposed to limit grain growth while achieving high density.[7,49] One of the largest reductions in κ was recently observed for consolidated solvothermal Bi_2Te_3 NPs with grain sizes of 10−100 nm and a porosity of ~10% with ~10 nm pore size.[43] Our as-prepared NPs had an average size of ~20 nm, but coarsened during consolidation. The average crystallite size from Rietveld refinement was 98 nm, indicating no significant peak broadening due to nanoscale crystallites. TEM measurements indicate that micrometer-sized grains are present alongside smaller grains (see Figure S8 in the Supporting Information). The grain growth is likely responsible for the relatively small drop in κ in our samples compared to previous reports. In addition, our samples had little porosity (density was more than 98% of that expected for Bi_2Te_3), which was important in the analysis of κ for Mehta et al.[43,50] A combination of small grain size and porosity may be required to further raise zT in these nanostructured thermoelectrics.

CONCLUSIONS

In summary, we demonstrate that the wet-chemical reaction of bismuth(III) oleate and TOP-Te with mild reaction temperatures and no additional surfactants can be used to synthesize stoichiometric Bi_2Te_3 NPs. Several critical factors, including temperature, solvent, and capping molecules, were identified as affecting the morphology of the resulting Bi−Te nanostructures. It is indicated that the relatively low temperature of 60 °C is beneficial for the formation of uniform single-crystalline spherical Bi_2Te_3 NPs with an average diameter of 20 nm. Higher temperatures favor the formation of platelike intergrown nanostructures with diameters ranging from several hundred nanometers to several micrometers. The formation of interpenetrating nanoplates is thermodynamically favorable and could be caused by the presence of lattice defects created during growth of the nanocrystals.[51,52] We employed a two-step ligand-exchange strategy based on nitrosonium tetrafluoroborate and hydrazine hydrate treatment to efficiently remove the organic surfactants from the surface of the as-synthesized Bi_2Te_3 NPs. The ability to reliably remove the organic surfactants from the surface of NPs significantly improves the TE properties of consolidated macroscopic samples. The maximum achieved zT at room temperature is 0.38, which is one of the highest reported values for nanostructured Bi_2Te_3 synthesized by wet-chemical approaches. The main challenge that remains to be solved to further increase the zT of chemically synthesized TE materials is to effectively prevent nanograin growth during consolidation and conserve nanoscale features and porosity for efficient phonon scattering.

ASSOCIATED CONTENT

Supporting Information

Additional characterization on Bi−Te and Bi NPs. This material is available free of charge via the Internet at http://pubs.acs.org.

AUTHOR INFORMATION

Corresponding Author

*E-mail: vnstavi@sandia.gov (V.S.); pasharm@sandia.gov (P.A.S.).

Notes

The authors declare no competing financial interest.

ACKNOWLEDGMENTS

We gratefully acknowledge financial support from the Sandia Laboratory-Directed Research and Development program. Sandia National Laboratories is a multi-program laboratory managed and operated by Sandia Corporation, a wholly owned subsidiary of Lockheed Martin Company, for the U.S. Department of Energy's National Nuclear Security Administration under Contract DE-AC04-94AL85000.

REFERENCES

(1) Tritt, T. M. In *Annual Review of Materials Research*; Clarke, D. R., Fratzl, P., Eds.; Annual Reviews: Palo Alto, CA, 2011; Vol. *41*, pp 433−448.
(2) Nolas, G. S.; Sharp, J.; Goldsmid, J. *Thermoelectrics: Basic Principles and New Materials Developments*; Springer: New York, 2011.
(3) Son, J. S.; Choi, M. K.; Han, M.-K.; Park, K.; Kim, J.-Y.; Lim, S. J.; Oh, M.; Kuk, Y.; Park, C.; Kim, S.-J.; Hyeon, T. *Nano Lett.* **2012**, *12*, 640−647.
(4) Xie, W.; He, J.; Kang, H. J.; Tang, X.; Zhu, S.; Laver, M.; Wang, S.; Copley, J. R. D.; Brown, C. M.; Zhang, Q.; Tritt, T. M. *Nano Lett.* **2010**, *10*, 3283−3289.
(5) Bux, S. K.; Fleurial, J.-P.; Kaner, R. B. *Chem. Commun.* **2010**, *46*, 8311−8324.
(6) Kanatzidis, M. G. *Chem. Mater.* **2009**, *22*, 648−659.
(7) Poudel, B.; Hao, Q.; Ma, Y.; Lan, Y. C.; Minnich, A.; Yu, B.; Yan, X. A.; Wang, D. Z.; Muto, A.; Vashaee, D.; Chen, X. Y.; Liu, J. M.; Dresselhaus, M. S.; Chen, G.; Ren, Z. F. *Science* **2008**, *320*, 634−638.
(8) Dresselhaus, M.; Chen, G.; Tang, M.; Yang, R.; Lee, H.; Wang, D.; Ren, Z.; Fleurial, J. P.; Gogna, P. *Adv. Mater.* **2007**, *19*, 1043−1053.
(9) Kim, C.; Kim, D. H.; Kim, H.; Chung, J. S. *ACS Appl. Mater. Interfaces* **2012**, *4*, 2949−2954.
(10) Wang, R. Y.; Feser, J. P.; Gu, X.; Yu, K. M.; Segalman, R. A.; Majumdar, A.; Milliron, D. J.; Urban, J. J. *Chem. Mater.* **2010**, *22*, 1943−1945.

(11) Scheele, M.; Oeschler, N.; Veremchuk, I.; Reinsberg, K.-G.; Kreuziger, A.-M.; Kornowski, A.; Broekaert, J.; Klinke, C.; Weller, H. *ACS Nano* **2010**, *4*, 4283−4291.
(12) Soni, A.; Zhao, Y. Y.; Yu, L. G.; Aik, M. K. K.; Dresselhaus, M. S.; Xiong, Q. H. *Nano Lett.* **2012**, *12*, 1203−1209.
(13) Saleemi, M.; Toprak, M. S.; Li, S.; Johnsson, M.; Muhammed, M. *J. Mater. Chem.* **2012**, *22*, 725−730.
(14) Chen, L.; Zhao, Q.; Ruan, X. *Mater. Lett.* **2012**, *82*, 112−115.
(15) Zhang, Y. C.; Wang, H.; Kraemer, S.; Shi, Y. F.; Zhang, F.; Snedaker, M.; Ding, K. L.; Moskovits, M.; Snyder, G. J.; Stuck, G. D. *ACS Nano* **2011**, *5*, 3158−3165.
(16) Dirmyer, M. R.; Martin, J.; Nolas, G. S.; Sen, A.; Badding, J. V. *Small* **2009**, *5*, 933−937.
(17) Scheele, M.; Oeschler, N.; Meier, K.; Kornowski, A.; Klinke, C.; Weller, H. *Adv. Funct. Mater.* **2009**, *19*, 3476−3483.
(18) Kovalenko, M. V.; Spokoyny, B.; Lee, J. S.; Scheele, M.; Weber, A.; Perera, S.; Landry, D.; Talapin, D. V. *J. Am. Chem. Soc.* **2010**, *132*, 6686−6695.
(19) Mi, J.-L.; Lock, N.; Sun, T.; Christensen, M.; Søndergaard, M.; Hald, P.; Hng, H. H.; Ma, J.; Iversen, B. B. *ACS Nano* **2010**, *4*, 2523−2530.
(20) Toprak, M.; Zhang, Y.; Muhammed, M. *Mater. Lett.* **2003**, *57*, 3976−3982.
(21) Altavilla, C.; Ciliberto, E. *Inorganic Nanoparticles: Synthesis, Applications, and Perspectives*; CRC Press: Boca Raton, FL, 2010.
(22) Schmid, G. *Nanoparticles: From Theory to Application*; Wiley-VCH, 2008.
(23) Pope, A. L.; Littleton, R. T.; Tritt, T. M. *Rev. Sci. Instrum.* **2001**, *72*, 3129−3131.
(24) Pope, A. L.; Zawilski, B.; Tritt, T. M. *Cryogenics* **2001**, *41*, 725−731.
(25) *Measurement Techniques and Considerations for Determining Thermal Conductivity of Bulk Materials*; Tritt, T. M., Weston, D., Eds.; Kluwer Academic: Dordrecht, The Netherlands, 2005.
(26) Bos, J. W. G.; Zandbergen, H. W.; Lee, M. H.; Ong, N. P.; Cava, R. J. *Phys. Rev. B* **2007**, *75*, 195203.
(27) Feutelais, Y.; Legendre, B.; Rodier, N.; Agafonov, V. *Mater. Res. Bull.* **1993**, *28*, 591−596.
(28) Yuan, Q.; Radar, K.; Hussain, M. M. *Chem. Commun.* **2011**, *47*, 12131−12133.
(29) Lu, W. G.; Ding, Y.; Chen, Y. X.; Wang, Z. L.; Fang, J. Y. *J. Am. Chem. Soc.* **2005**, *127*, 10112−10116.
(30) Zheng, Y. Y.; Zhu, T. J.; Zhao, X. B.; Tu, J. P.; Cao, G. S. *Mater. Lett.* **2005**, *59*, 2886−2888.
(31) Wang, Z.; Wang, F. Q.; Chen, H.; Zhu, L.; Yu, H. J.; Jian, X. Y. *J. Alloys Compd.* **2010**, *492*, L50−L53.
(32) Zhao, X. B.; Ji, X. H.; Zhang, Y. H.; Zhu, T. J.; Tu, J. P.; Zhang, X. B. *Appl. Phys. Lett.* **2005**, 86.
(33) Jiang, L.; Zhu, Y. J.; Cui, J. B. *Eur. J. Inorg. Chem.* **2010**, 3005−3011.
(34) Deng, Y.; Wei, G. D.; Nan, C. W. *Chem. Phys. Lett.* **2003**, *368*, 639−643.
(35) Hu, J. Z.; Zhao, X. B.; Zhu, T. J.; Zhou, A. J. *Phys. Scr.* **2007**, *2007*, 120.
(36) Teweldebrhan, D.; Goyal, V.; Balandin, A. A. *Nano Lett.* **2010**, *10*, 1209−1218.
(37) Deng, Y.; Zhou, X.-S.; Wei, G.-D.; Liu, J.; Nan, C.-W.; Zhao, S.-J. *J. Phys. Chem. Solids* **2002**, *63*, 2119−2121.
(38) Zhao, X. B.; Ji, X. H.; Zhang, Y. H.; Cao, G. S.; Tu, J. P. *Appl. Phys. A: Mater. Sci. Proces.* **2005**, *80*, 1567−1571.
(39) Peng, X. G.; Wickham, J.; Alivisatos, A. P. *J. Am. Chem. Soc.* **1998**, *120*, 5343−5344.
(40) Johnson, I.; Mer, V. K. L. *J. Am. Chem. Soc.* **1947**, *69*, 1184−1192.
(41) Dong, A.; Ye, X.; Chen, J.; Kang, Y.; Gordon, T.; Kikkawa, J. M.; Murray, C. B. *J. Am. Chem. Soc.* **2010**, *133*, 998−1006.
(42) Goldsmid, H. J. *Proc. Phys. Soc. London* **1958**, *72*, 17−26.
(43) Mehta, R. J.; Zhang, Y. L.; Karthik, C.; Singh, B.; Siegel, R. W.; Borca-Tasciuc, T.; Ramanath, G. *Nat. Mater.* **2012**, *11*, 233−240.
(44) Jonker, G. H. *Philips Res. Reports* **1968**, *23*, 131-&.
(45) Goldsmid, H. J.; Sheard, A. R.; Wright, D. A. *J. Appl. Phys.* **1958**, *9*, 365−369.
(46) Cope, R. G.; Penn, A. W. *J. Mater. Sci.* **1968**, *3*, 103−109.
(47) Fleurial, J. P.; Gailliard, L.; Triboulet, R.; Scherrer, H.; Scherrer, S. *J. Phys. Chem. Solids* **1988**, *49*, 1237−1247.
(48) Yarden, T. S.; Joselevich, E. *Nano Lett.* **2010**, *10*, 4742−4749.
(49) Aabdin, Z.; Peranio, N.; Eibl, O.; Tollner, W.; Nielsch, K.; Bessas, D.; Hermann, R.; Winkler, M.; Konig, J.; Bottner, H.; Pacheco, V.; Schmidt, J.; Hashibon, A.; Elsasser, C. *J. Electron. Mater.* **2012**, *41*, 1792−1798.
(50) Mehta, R. J.; Karthik, C.; Singh, B.; Teki, R.; Borca-Tasciuc, T.; Ramanath, G. *ACS Nano* **2010**, *4*, 5055−5060.
(51) Mandal, T.; Piburn, G.; Stavila, V.; Rusakova, I.; Ould-Ely, T.; Colson, A. C.; Whitmire, K. H. *Chem. Mater.* **2011**, *23*, 4158−4169.
(52) Mandal, T.; Stavila, V.; Rusakova, I.; Ghosh, S.; Whitmire, K. H. *Chem. Mater.* **2009**, *21*, 5617−5626.